

Mitigation of flow induced vibration of head gimbal assembly

Qi De Zhang · Chok Shiong Tan · Kannan Sundaravadivelu ·
Maria A. Suriadi · Gim Leong Chin · Teck Hong Yip ·
Eng Hong Ong · Ning Yu Liu

Received: 29 July 2008 / Accepted: 22 January 2009 / Published online: 31 March 2009
© Springer-Verlag 2009

Abstract The airflow of a 10,000 rpm hard disk drive is simulated using the LES turbulent model. The critical parameters for using LES model to get the correct/reliable result are discussed. The flow induced vibration of the head gimbal assembly is calculated with the obtained fluid force acting on the head gimbal assembly (HGA) and compared with measured results. Good agreement is observed between the measured and simulated results. The optimization of the airflow is further carried out to reduce the flow induced vibration of the HGA. It is found that almost 50% reduction of flow induced vibration of the HGA can be achieved with the proposed modifications for airflow optimization.

1 Introduction

The recording density of hard disk drives (HDDs) is increasing 60% every year targeting 1 Tb/in² by 2012 (Frank and Wood 2006). In order to meet up with this increasing trend the positioning accuracy of the magnetic head must be significantly improved for both in-plane and out-of-plane directions. However, the flow-induced vibration of the head gimbal assembly (HGA) causes track misregistration and limits the track density. Therefore it is important to understand the mechanism of flow-induced vibration and reduce it by optimizing the airflow of hard disk drives.

Many researchers have investigated airflow and flow induced disk flutter and head gimbal assembly vibration by numerical simulation or experimental measurement as reported by Humphrey et al. (2002), Shimizu et al. (2003), Tsuda et al. (2003), Nakamura et al. (2005), Aruga et al. (2007), and Zhang et al. (2008).

Recently Ikegawa et al. (2006) investigated the air flow pattern changes in a HDD through the introduction of a bypass and a spoiler with the LES model and compared their numerical results with the measurements using particle image velocimetry (PIV). Their analyses revealed that the introduction of a spoiler decreases the flow velocity near the arm by decreasing average flow velocity between the disks such as diverting the flow into the bypass channel, and by moving the high-speed-flow area toward the inner-radius area of the disks. They concluded that the arm vibration could be reduced by 30% with these modifications.

Tan and Suriadi (2007) numerically investigated the effect of flow induced vibration with and without weight saving holes on the actuator and found that the displacement of the arm tip is dominated by the first bending natural frequency. The weight saving holes are beneficial for control but they increase the roll displacement of the arm. Covering the weight saving holes improves the first bending natural frequency but increases the out-of-plane vibration due to the increase of out-of-plane torque.

Kazemi and Tokuda (2007) investigated the slider off-track vibration in a 3.5 inch, 10,000 rpm disk drive. The aerodynamic loads on the different components of the HGA were calculated and the transient response of the HGA was obtained. It was found that the slider off-track vibration is dominated by the first torsion of the suspension.

In continuation to these investigations a numerical attempt has been made in this paper to investigate the

Q. D. Zhang (✉) · C. S. Tan · K. Sundaravadivelu ·
M. A. Suriadi · G. L. Chin · T. H. Yip · E. H. Ong · N. Y. Liu
Data Storage Institute, DSI Building, 5 Engineering Drive 1
(off Kent Ridge Crescent, NUS), Singapore 117608, Singapore
e-mail: ZHANG_Qide@dsi.a-star.edu.sg

flow-induced vibration of the HGA in a 10,000 rpm HDD. The fluid force is obtained by numerical simulation, then the vibration of the HGA is calculated using the obtained fluid force. The predicted vibration results are compared with the experimental measurements. Good agreement is observed between the predicted and measured results. Then the effect of using different flow optimizing devices to reduce the flow induced vibration is further investigated. It is found that with the proposed modification, the flow induced vibration can be reduced around 50%.

2 Model and simulations

A commercially available 10,000 rpm disk drive is selected for the investigation and the model is built by reverse engineering as shown in Fig. 1a. We start the investigation with the whole disk drive including all components. Some important parameters of the model are: 1.5 million tetrahedral cells are used for fluid volume; no slip condition is applied at all walls; Dynamic Smagorinsky-Lily Sub-grid Large Eddy Simulation model is used for turbulent model and the time step is 10 μ s.

Like many recently published papers, the LES model is used in this investigation. The choice of using LES model instead of RANS models (such as k - ε model or RSM model) is based on the following considerations: (1) RANS models

provide time-averaged results but LES provides instantaneous information which is needed for HGA transient vibration analysis, (2) RANS models over-predict the turbulent kinetic energy in regions such as flow impingement and re-attachment regions, (3) RANS models cannot accurately predict highly swirling flow (Pope 2000). Consequently, RANS models cannot give us accurate predictions of flow forces on the arm and the suspension of disk drives. Hence, the LES model is preferred although it needs much more computing resources than RANS models do.

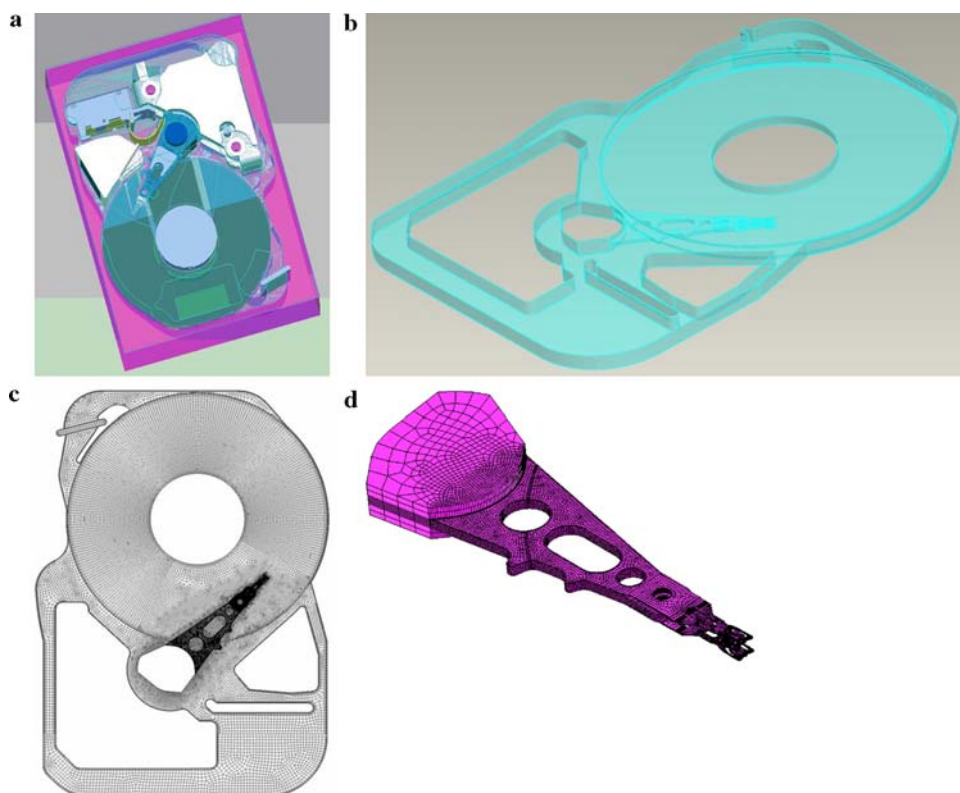
LES model is supposed to provide us time-varying and improved prediction of flow forces. However, if it is used improperly, the LES model could not give us better results than those obtained by RANS models. Hence, it is important to check the result with some important criteria to make sure that the obtained results are reliable. The important parameters should be checked and make sure that they meet certain criteria are: time step size, non-dimensional wall distance y^+ , and the percentage of resolved turbulent eddies.

For the above mentioned whole disk drive model, the time step size (10 μ s) used in the simulation is first checked. Using the Taylor's microscale, we have

$$\tau = 15\gamma/\varepsilon^{1/2} \approx 1.14 \times 10^{-5}(\text{s}) \quad (1)$$

where γ is the kinetic viscosity of air and ε is the turbulence dissipation rate. We can use RANS model result for this

Fig. 1 Disk drive, 3D models and meshes. **a** Built 3D model. **b** Investigation region of the refined model. **c** Mesh of numerical model for flowfield. **d** Mesh of HGA for structure analysis



estimation. Equation 1 correctly characterizes the time-scale of very small eddies that are responsible for the dissipation of the energy. This calculated timescale is almost 4 times higher than the Kolmogorov time scale and hence is acceptable for the use in LES simulation.

However the maximum value of y^+ is 47.5 and only 45% of the turbulent eddies is resolved. This reveals that the meshes near wall are too coarse and the resolved turbulent energy is much <80%, hence, cannot be considered as a fine LES. Therefore the mesh of the model must be refined to produce improved prediction.

Based on the full model result and the consideration of computing resource needed, we select a refined model which only considers the region between two co-rotating disks. The settings of the refined model are: a slice of the air domain between two rotating disks is used in this study as shown in Fig. 1b. The model dimensions: the disk diameter is 84 mm, the spacing between the two disks is 2.4 mm, the arm thickness is 1.1 mm and the actuator is at the middle diameter (MD) position during the simulation.

The rotational Reynolds number is $Re_\Omega = 1.26 \times 10^5$ and $Re_n = 3288$, based on the disk radius and the half spacing between two disks, respectively. Using the rotational Reynolds number, the different Kolmogorov scales, that is, the length, time and velocity scales are then estimated again. With reference to the length scales a fully structured mesh for flow domain and a fully structured viscous or boundary layer mesh on all surfaces is constructed in such a way that 80% of the total eddy scales is resolved thus ensuring that the present LES calculations are carried out on a sufficiently fine mesh. This amounted to a total number of 1.7 million grid cells in the whole fluid domain (Fig. 1c). The first computational cell next to each of the walls is found at $y^+ < 1$, the maximum $y^+ = 1.8$ for the whole model and almost 80% of turbulent eddies is resolved for the new model. As it is well known that to produce a good LES with fine near-wall resolution we need to ensure that the filter and grid are sufficiently fine to resolve 80% of the energy everywhere and the dimensionless wall distance, that is, the y^+ has to be around unity (Pope 2000). These requirements are met by the above refined mesh model. Totally, there are 41 unevenly distributed nodes in Z direction between the two disks, which results in the minimum $\Delta z = 0.02$ mm and the maximum $\Delta z = 0.105$ mm. Hence, the model is considered acceptable for a good LES.

The governing equations are discretized using finite volume method (FVM). The spatial and time derivatives are approximated using bounded central-differencing and second order upwind discretization schemes. The time step size used in this study is still 10 μ s, close to the estimated time scale of 11 μ s. Thus for the simulation of one complete disk revolution 600 time steps are required. The

initial condition to start LES is obtained by perturbing a converged RANS model solution. Thereafter transient computations were carried out for 60 ms (10 revolutions) so as to allow the flow become statistically steady. After the flow becomes statistically steady, the transient data of the fluid force and flow variables are collected at each time step for 30 ms (five revolutions), so as to perform the statistical analysis. Structural analysis input data is generated using an in-house developed code.

Subsequently the input conditions are fed into a FEM code for calculating the actuator and suspension vibration. The FEM model constructed consists of around 140,000 fully structured meshed solid elements as shown in Fig. 1d. The fluid forces acting on the surface nodes of the actuator and suspension assembly are extracted from the CFD solver and then mapped onto the surface nodes of the respective solid elements. Full transient structural analysis using the improved Newmark time integration method is performed to obtain the displacement of the HGA. The settings for the vibration analysis are: around 140,000 fully structured mesh; time varying pressure and viscous/fluid shear forces applied on all components of HGA; 3 DOF constraints on pivot bottom surface; Constraint equations to emulate contact/bonding between various actuator parts; Link element with constraint equation to represent dimple-gimbal contact; Linear spring-damper elements to represent the slider air bearing; Frictionless contact between slider and disk. Time step size is 10 μ s and the duration is 30 ms (five revolutions). The material properties for the vibration analysis are listed in Table 1.

3 Results and discussion

Figure 2a–c show the velocity field, pressure distribution and vortices at the mid-plane of the drive. It is observed that flow speed becomes slower before the fluid approaches

Table 1 Material properties for structure analysis

Aluminum (Arm)	Young's modulus	69 GPa
	Density	2,710 kg/m ³
	Poisson's ratio	0.33
Steel (Load beam, Hinge, Gimble)	Young's modulus	210 GPa
	Density	8,700 kg/m ³
	Poisson's ratio	0.30
Ceramic (Slider)	Young's modulus	410 GPa
	Density	4,350 kg/m ³
	Poisson's ratio	0.30
Kapton (FlexCable)	Young's modulus	3 GPa
	Density	1,574 kg/m ³
	Poisson's ratio	0.30

the arm; then accelerates along the arm and suspension (Fig. 2a). There is less air mass that flows into the VCM region through the air path channel. The pressure before the arm is obviously higher than that after the arm. Corresponding to the acceleration of airflow, the pressure is lower at that region as shown in Fig. 2b. There are many vortices behind the arm and the suspension (Fig. 2c). The flow induced vibration of the HGA is the integrated effect of these flow forces.

To distinguish the effect of different fluid forces, the fluid forces acting on the arm and suspension are separated into the pressure force and the viscous force with following formula:

$$F_a = \vec{a} \cdot \vec{F}_p + \vec{a} \cdot \vec{F}_v \quad (2)$$

where \vec{a} is the specified vector; \vec{F}_p is pressure force vector; \vec{F}_v is viscous force vector; F_a is total force component; $\vec{a} \cdot \vec{F}_p$ is pressure force component; $\vec{a} \cdot \vec{F}_v$ is viscous force component. After separation, checking the forces acting on the different components of the HGA, it is found that the percentage of fluctuation contributed by the viscous force to the total force increases as the position moves from the arm towards the suspension tip as shown in Table 2.

Using the obtained fluid force, the flow induced vibration is calculated. The predicted vibration shows around 60 nm peak to peak value in the vertical direction, taken from the tip of the suspension (Fig. 3a). The measured vibration amplitude shows almost 50 nm peak to peak value, measured at the tip of the suspension also (Fig. 3b). Average at frequency domain, the predicted vibration of repeatable run out (RRO) is 61.9 nm while the measured value of RRO is 48.9 nm. The predicted highest peak is at $f = 1,040$ Hz with amplitude of 3.53 nm. For measured result, there is a peak at $f = 1,090$ Hz with amplitude of 3.41 nm as shown in Fig. 3c and d. The possible reasons for the discrepancy between the measurement and the simulation results are: (1) the material properties used for the simulation is not exactly representing the real components material properties; (2) the stiffness of ABS used in the simulation is lower than that of the real one. It is also observed that in the frequency domain, the measured result is much “cleaner” i.e. fewer peaks than that of the predicted result. This is because the measurement result is averaged with the data of more than 5,000 disk revolutions but the simulation only collected the data for five disk revolutions. However, the comparison shows that, in general, our simulation agrees with the measurement result. Therefore, we can further investigate how to reduce the FIV using the same approach introduced in the previous sections.

Since the total transient force on the HGA consists of fluctuating pressure and viscous forces, and pressure force is related to the rate of airflow mass, viscous force is the

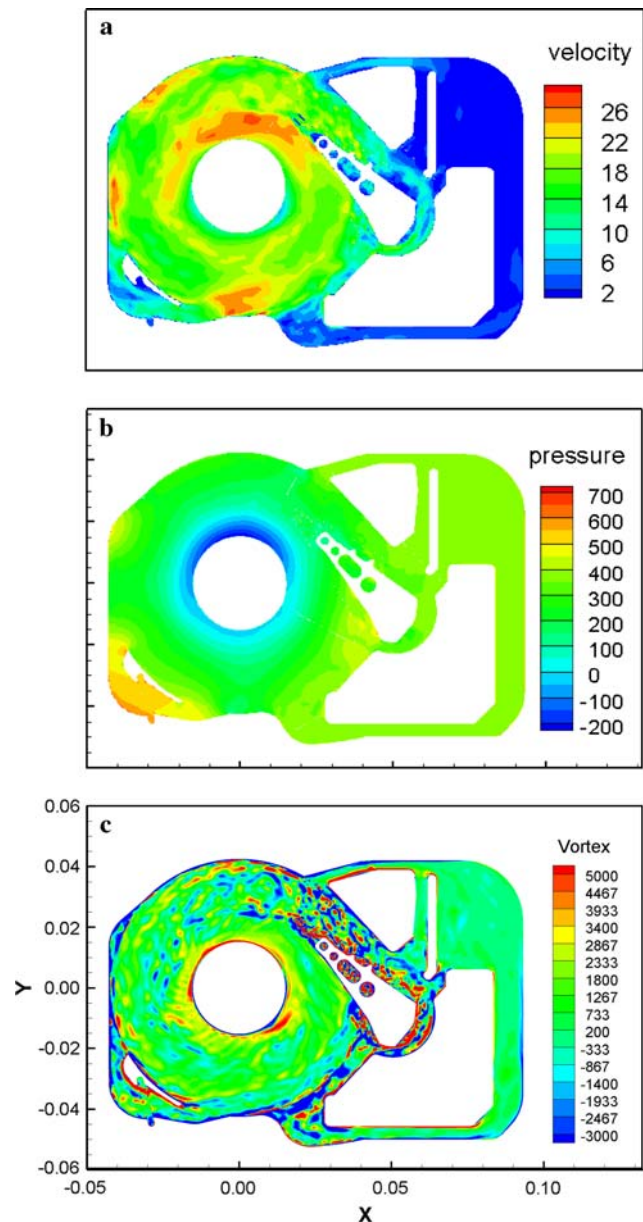


Fig. 2 Velocity magnitude, pressure distribution and vortices at the mid-plane ($z = 0$) between the two disks of original model (M1). **a** Velocity magnitude (m/s) in the mid-plane of two co-rotating disks. **b** Pressure distribution (Pa) in the mid-plane of two co-rotating disks. **c** Instantaneous axial velocity contours at mid-plane of two co-rotating disks. Red Upward; Blue Downward, Each blue and red pair forms a vortex pair (1/s)

combination of laminar viscous force and the vortex shedding force. To reduce vibration caused by these two different type forces, different approaches are required. To reduce the pressure force, airflow rate should be reduced by means of blocking, diverting, etc. so that the flow mass passing the actuator arm and suspension is reduced. To reduce the vortex force, the vortex scale should be reduced. Hence, splitting flow into multiple channels by adding splitter behind the suspension can be used.

Table 2 Percentage of viscous force in total fluid force on HGA components

	Force X (%)	Force Y (%)	Force Z (%)
Arm-Susp. Assembly	18.41	9.38	2.79
Arm only	17.51	8.28	2.72
Bottom Susp. Assembly	51.14	33.84	3.65
Bottom Susp. Loadbeam	72.90	37.64	9.00
Bottom Susp. Flex cable @ Slider	61.74	68.97	14.20
Bottom slider	7.79	4.46	9.61

Based on the above-mentioned considerations, two modifications to the original disk drive are introduced as shown in Fig. 4b, c for the mitigation of flow-induced vibration. Modifications made in model 2 are: (1) adding the flow diverter before the arm to force the airflow into the bypass, (2) enlarging the flow path to allow more air to pass it, and (3) blocking the flow at vertical flex cable area to reduce the pressure fluctuation caused vibration of the flex cable (Fig. 4b). In addition to the modifications made in model 2, the downstream spoilers are added behind the sliders in model 3 to reduce the viscous fluctuation force as shown in Fig. 4c. The thickness of the spoiler is 0.3 mm, three such spoilers are inserted into the space between the two rotating disks in the way that the middle planes of the top and the bottom spoilers are aligned to the middle plane of two sliders in Z (vertical) direction and the middle spoiler is aligned with the center plane between the two disks.

Figure 5 compares the flow field, pressure distribution and vortices of two modified models (M2 and M3). Compared with results of model 1 (Fig. 2a–c), it is found that a

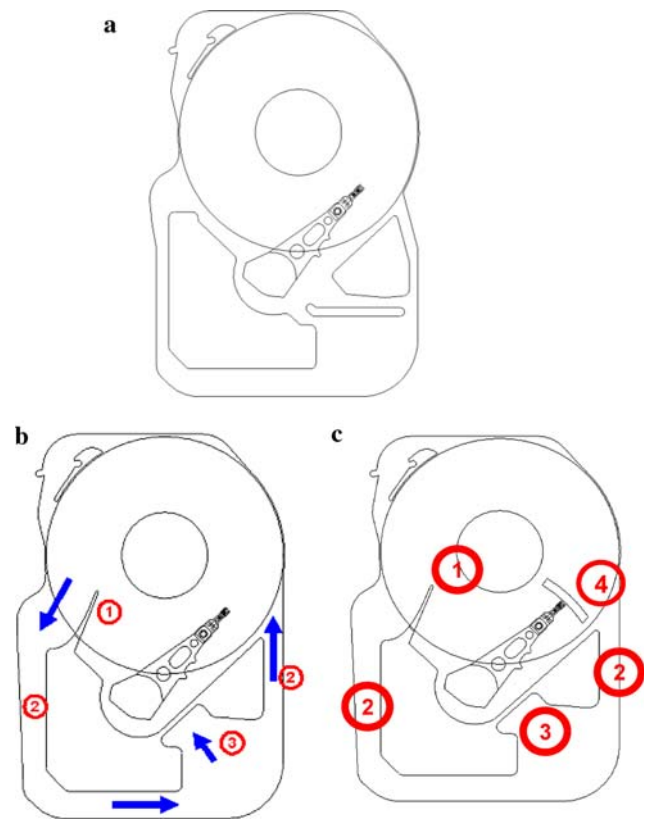


Fig. 4 Schematic drawing of model modifications. **a** Model 1 (Original HDD). **b** Model 2 (Modification 1). **c** Model 3 (Modification 2)

larger amount of air flow is diverted into the bypass channel thus reducing the magnitude of the aerodynamic forces acting on the entire arm unit. Consequently, the vibration of HGA is obviously reduced with the modifications of model 2 as anticipated. It is also expected that the configuration with the bypass, the diverter and the

Fig. 3 Simulated and measured vibration of suspension tip in time and frequency domains. **a** Simulated vibration of suspension tip in time domain. **b** Measured vibration of suspension tip in time domain. **c** Simulated vibration of suspension tip in frequency domain. **d** Measured vibration spectrum of suspension tip in frequency domain

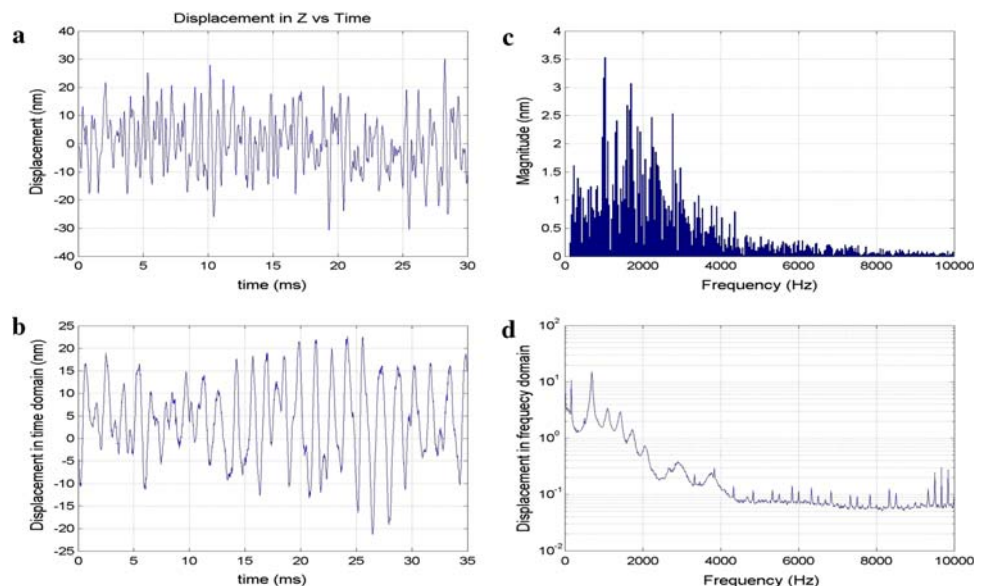


Fig. 5 Comparison of flow field and pressure changes in different models. **a** Velocity (m/s) of modified model (M2). **b** Velocity (m/s) of modified model (M3). **c** Pressure (Pa) of modified model (M2). **d** Pressure (Pa) of modified model (M3). **e** Vortex (1/s) of modified model (M2). **f** Vortex (1/s) of modified model (M3)

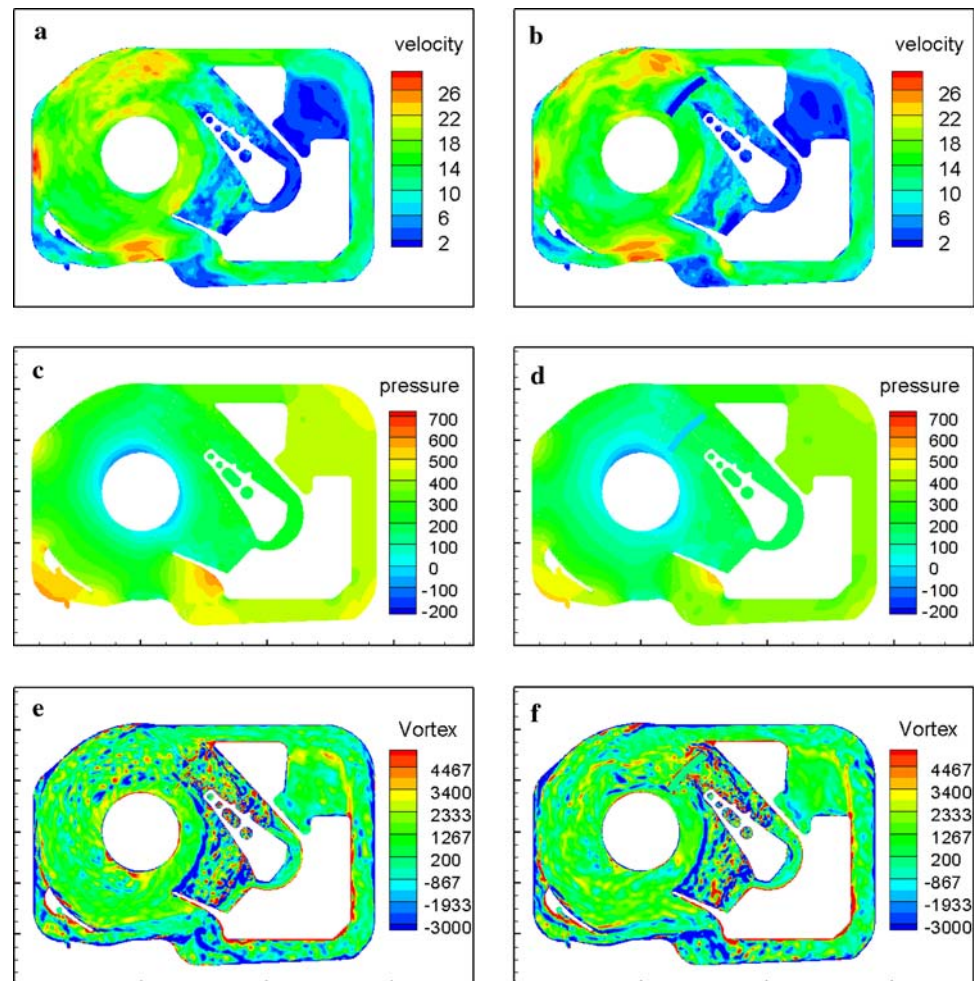


Table 3 Comparison of vibration amplitude improvement measured at the suspension tip

	Original	After modification	
Vibration	M1 (nm)	M2 (nm)	M3 (nm)
In-plane	10.70	5.55	3.00
Out-of-plane	66.62	29.77	32.11
Improvement			
M2	In plane	5.55 nm	48% reduction
	Out-of-plane	29.77 nm	55% reduction
M3	In plane	3.00 nm	71% reduction
	Out-of-plane	32.11 nm	51% reduction

splitter (model 3) will further reduce the HGA vibration by reducing the viscous force acting on the suspension due to the vortex shedding. However, the results of model 3 show that adding splitter after the suspension also increases the pressure fluctuation. Consequently, the in-plane vibration is reduced and the out-of-plane vibration is slightly increased compared with the results of model 2.

The vibration amplitude for the above-mentioned 3 cases are listed and compared in Table 3. It is observed that the proposed flow diverter and the vortex splitter can suppress the FIV around 50% for both in-plane and out-of-plane vibrations.

4 Conclusions

The numerical simulation of flow-induced HGA vibration of disk drive is carried out. Agreement between the results of simulation and measurement is observed. The simulation results show that the out-of-plane vibration is mainly caused by the turbulent pressure fluctuation and the in-plane vibration is mainly caused by the viscous force.

To investigate the effect of flow optimizing devices, a flow diverter and a vortex splitter in between the disks region and in the neighborhood of the slider region are introduced to attenuate air turbulence so that the HGA vibration can be reduced. The simulations show that the proposed flow regulator and the vortex splitter can suppress

the flow induced vibration by 50% for both in-plane and out-of-plane vibrations.

These results are substantiated by calculating the corresponding displacement of the slide in all the three directions. It is inferred that the magnitude of slider vibration is reduced largely in the presence of the modified flow configuration by means of the diverter-bypass and the vortex splitter.

For better comparison of simulation and measurement results, a longer time collection of simulation data is needed. However, simulations with LES model requires significant computing resource and quite long calculating time, hence, exploration for a more efficient approach or turbulent models is needed for the flow induced vibrations in high speed rotating devices.

References

- Aruga K, Suwa M, Shimizu K, Watanabe T (2007) A study on position error caused by FIV using helium filled hard drives. *IEEE Trans Magn* 43(9):3750–3755
- Frank P, Wood R (2006) A perspective on the future of hard disk drive (HDD) Technology. APMRC 2006, Singapore, FB-01
- Humphrey JAC, Haj-Harir H, Iwasaki T, Kazemi M, Rosales L (2002) Modeling and controlling flow induced suspension-head unit vibrations in hard disk drives. *Microsyst Technol* 8(6):375–382
- Ikegawa M, Hirono Y, Mukai H, Kaiho M (2006) Decreasing airflow velocity in hard disk drives with a spoiler and bypass. *IEEE Trans Magn* 42(10):2594–2596
- Kazemi M, Tokuda A (2007) An investigation on flow-induced off-track vibration of head gimbal assemblies in hard disk drives. ISPS 2007, USA, SAFV-A3
- Nakamura S, Aduma R, Takahashi H, Wakatsuki K, Hagiya S (2005) Flow induced vibration of a head gimbal assembly under various conditions. *IEEE Trans Magn* 41(2):769–773
- Pope SB (2000) *Turbulent flows*. Cambridge University Press, Cambridge
- Shimizu H, Shimizu T, Tokuyama M, Masuda H, Nakamura S (2003) Numerical simulation of positioning error caused by air-flow-induced vibration of head gimbals assemble in hard disk drive. *IEEE Trans Magn* 39(2):806–811
- Tan CS, Suriadi MA (2007) Flow induced vibration caused by weight-saving hole on actuator arm using large eddy simulation. ISPS 2007, USA, SAFV-B4
- Tsuda N, Kubotera H, Tatewaki M, Noda S, Hashiguchi M, Maruyama T (2003) Unsteady analysis and experimental verification of the aerodynamic vibration mechanism of HDD arms. *IEEE Trans Magn* 39(2):819–825
- Zhang QD, Yip TH, Guo GX (2008) Flow-induced vibration in hard disk drives. *Int J Prod Dev* 5(3–4):390–409